CHINESE OPTICS LETTERS

Vol. 23, No. 1 | January 2025

Optical fiber fluorescence probe for chloride ion detection based on graphitic carbon nitride quantum dot-doped hydrogel

Xia Li (李 霞)[1], Sicheng Ke (柯思成)[1], Chenxiao Wang (王晨晓)[1], Wa Jin (金 娃)[1], Xinghu Fu (付兴虎)[1], Guangwei Fu (付广伟)[1], and Weihong Bi (毕卫红)[1,2*]

[1] School of Information Science and Engineering, Key Laboratory for Special Fiber and Fiber Sensor of Hebei Province, Yanshan University, Qinhuangdao 066004, China

[2] Zhongshan Institute of Changchun University of Science and Technology, Zhongshan 528400, China

*Corresponding author: bwhong@ysu.edu.cn

Received April 18, 2024 | Accepted July 17, 2024 | Posted Online February 4, 2025

We conducted an experimental study on an off-on fluorescence optical fiber probe utilizing graphitic carbon nitride quantum dots (g-CNQDs) -doped hydrogel for chloride ion detection. It resulted in fluorescence quenching after g-CNQDs were modulated by silver ions (Ag^+). The chloride ion sensing probe was obtained by wrapping the tapper fiber tip with the composite fluorescent material of g-CNQDs/Ag^+ mixed with chitosan hydrogel. Within the concentration range of 1–9 μM chloride ions, the fluorescence intensity of the prepared optical fiber probe exhibits a robust linear correlation with chloride ion concentration, and the detection limit is 0.037 μM.

Keywords: optical fiber probe; carbon nitride dot; chloride ion; off-on fluorescence.
DOI: 10.3788/COL202523.010603

1. Introduction

Chloride ion (Cl^-) is involved in various physiological processes in the physiological system and is widely distributed in nature, and it is also considered to be the signature ion of cystic fibrosis[1]. At the same time, chloride ions are among the most prevalent ions in liquid water environments and are an important parameter in water quality monitoring. Chloride ion is the main component of salt spray and the main cause of salt spray corrosion[2]. A large amount of chloride ion deposition will lead to metal corrosion, concrete erosion and damage, and fresh water and soil salinization will affect crop yield[3]. Excessive chloride ions have many harmful effects on the environment and physiology, so the detection of chloride ions is very important. Traditional detection methods include the electrochemical method[4], chromatography[5], laser-induced breakdown spectroscopy[6], colorimetry[7], and the Mohr method[8]. However, these methods have some limitations, such as complex operation, inability to achieve real-time on-line detection, inability to detect trace chloride ions, and low sensitivity. Hence, discovering a simple and effective detection method holds great significance.

In recent years, more and more attention has been paid to the fluorescence method due to its advantages of low cost, sensitivity, simple operation, and simplicity. Due to the strong affinity between the chloride ion and the silver ion, chloride is used as a fluorescent chemical sensor to detect chloride ions. Kim *et al.*[9] proposed a fluorescent chemical sensor for the detection of chloride ions through ligand displacement of Ag^+-benzimidazole complexes. This method demonstrated that the detection limit was 19 μM, and the response time was 3 min. Yue *et al.*[10] prepared an Ag-carbon quantum dot fluorescence complex with an "off-on" mechanism for chloride ion detection, and its detection limit was 2.817 μM. Fluorescent molecules with a strong hydrogen bond structure are used as fluorescent probes for chloride ion detection[11]. Jeong *et al.*[12] prepared a spiral array folding body fluorescence molecule based on indole carbazole, using indole as a hydrogen bond acceptor to bind chloride ions. Li *et al.*[13] synthesized tetraphenyl triazole ring sweet compound as a chloride fluorescence indicator. Its structure has a large ring cavity and is beneficial because of the hydrogen bond that is in the direction of two dimensions and the halogen ion 1:1 complexation to its fluorescence enhancement. Because the central cavity and halogen ions are high, this kind of fluorescent probe has the ability to specifically recognize the chloride ion. Fluorescent fiber-optic probes, which combine fluorescent materials with optical fibers, are also widely used for the detection of Cl^-. Wu *et al.*[14] immobilized cellulose acetate-doped silica nanoparticles on the end face of an optical fiber for the detection of Cl^-. Ding *et al.*[15] used glossiness as a fluorescent indicator for chloride ions

and immobilized it on the inner surface of a suspended core optical fiber for the detection of Cl^-.

g-CNQDs possess notable benefits of good biocompatibility, excellent thermal stability, non-toxicity, and great chemical stability. These properties make them highly promising for diverse applications in environmental protection, new energy, drug delivery, cancer treatment, sensing, and other fields[16]. Chen *et al.*[17] integrated g-CNQDs with horseradish peroxidase for the detection of hydroquinone, achieving an impressively low detection limit of 0.04 μM. Liu *et al.*[18] developed an open-type fluorescent nanocomposite based on Cu^{2+}-g-CNQDs to test the adenylate kinases with a limit of detection as low as 0.06 U/L. Ghasem *et al.*[19] prepared a g-C_3N_4 with a rich carboxyl serving to be a selective material for a Hg^{2+} and Fe^{3+} test, which showed detection limits of 12 nm and 190 nM, respectively. Therefore, g-CNQDs nanofluorescent materials can provide an opportunity for the detection of chloride ions.

In this Letter, we proposed a fiber optic fluorescence sensor based on g-CNQDs/Ag^+ -doped hydrogel to test Cl^- ions utilizing the "off–on" mechanism. The g-CNQDs/Ag^+ were fixed in chitosan hydrogel, which maintained the optical characteristics for g-CNQDs/Ag^+ in a solution and could penetrate the external analyses well. The fluorescence of the g-CNQDs will be quenched through photoelectron transfer mechanism between g-CNQDs and silver ions. When chlorine ions are added, the binding energy between chloride ions and silver ions is stronger, so silver ions are separated from the g-CNQDs, and part of the fluorescence of the g-CNQDs is restored. The experimental results indicate that the linear correlation between fluorescence recovery of the g-CNQDs and the concentration of the chloride ion is in the range of 1–9 μM.

2. Experiment

g-CNQDs were purchased from the Yanshan University. Chitosan (CS, viscosity of 400 mPa.s), acetic acid (5%), Glyoxal (40%), silver nitrate ($AgNO_3$), sodium hydroxide (NaOH, 1 mol/L), anhydrous ethanol, (3-aminopropyl)-triethoxysilane (APTES), sulfuric acid (H_2SO_4), and hydrogen peroxide (H_2O_2) were supplied from Macklin. Hydrofluoric acid (HF, 40%) and paraffin were supplied from Sinopharm Chemical Reagent Co. Ltd. The multimode fibers (MMFs) (core diameter 105 μm, cladding diameter 125 μm) were purchased from Fiberhome. All reagents do not need additional processing.

The g-CNQDs-Ag^+ were prepared using the cross-linking method, where 3 mg of g-CNQDs were taken and mixed with 50 ml of Milli-Q water. This mixture was then placed in an ultrasonic shaker and shaken continuously for 2 h to ensure that the g-CNQDs would be evenly dispersed in the water. Then, 2 mL of g-CNQD dispersion was mixed with 100 μl (500 μmol/L) of $AgNO_3$, which served here to introduce Ag^+ to interact with the g-CNQDs, and ultrasonic shaking was continued for 1 h to form g-CNQDs-Ag^+ composites. The CS/g-CNQDs-Ag^+ composite films were prepared as follows: 0.02 g of CS was dissolved in 10 mL of Milli-Q water containing 1 mL of acetic acid

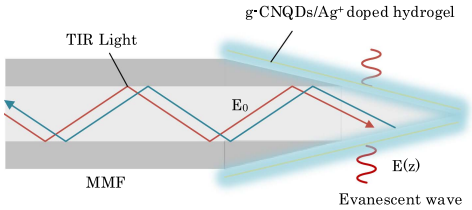

Fig. 1. Schematic of the probe structure.

to enhance the solubility of the chitosan, and stirred for 1 h at 50°C. The pH of the solution was then adjusted to neutral with NaOH. Finally, 1 ml of the previously prepared g-CNQDs-Ag^+ composite solution and 100 μl of glyoxal were added to the chitosan solution that had been adjusted to neutral, where glyoxal acted as a cross-linking agent to enhance the mechanical strength and stability of the composite membrane.

The fiber probe consists of an MMF with a conical tip, the surface of which is coated with a g-CNQDs/Ag^+-doped hydrogel, as illustrated in Fig. 1. The principle of the probe depends on the evanescent wave (EW) principle and fluorescence effect.

According to the Fresnel formula[20], as the beam of light transitions from an optically dense medium enters an optically rare medium, when the angle of incidence is larger than the critical angle, there is total internal reflection, and all light rays return to the optically dense medium. The index of refractive of the fiber core is greater than that of the cladding, so the beam propagates by total reflection in the fiber, but because the Fresnel coefficients of the transverse electric field and transverse magnetic field are not zero, this means that although the light energy is fully reflected, the electromagnetic field can leak into the optically phobic medium. The evanescent wave decays exponentially, and the evanescent wave amplitude at z is

$$E(z) = E_0 \exp(-z/d_p), \tag{1}$$

where $E(z)$ is the amplitude of the evanescent wave at z, z is the distance from the interface of the fiber optic probe, d_p is the penetration depth, and E_0 is the amplitude of the electromagnetic field at the interface.

The penetration depth d_p, defined as the distance where the strength of the electromagnetic field is 1/e of the electromagnetic strength of the interface, can be written as

$$d_p = \frac{\lambda}{\sqrt{2\pi(n_1^2 \sin^2\theta - n_2^2)}}, \tag{2}$$

where n_1 and n_2 are the dense and rare media refractive indices, respectively, λ is the incident light wavelength, while θ is the angle between the incident light and normal light.

Because the evanescent wave can excite the fluorescent material existing on the surface of the fiber, and obtained signal is also directly correlated to the interaction of the material to be tested, the rapid and real-time response to the sample composition can be observed. The obtained results reveal that the fluorescence intensity varies with the concentration of chloride ions, and chlorine can be determined according to the theory of

fluorescence quenching. The theoretical equation for the Stern–Volmer quenching is

$$I_0/I = 1 + K_S[C], \tag{3}$$

where I_0 is the initial fluorescence intensity without quenching, I is the intensity of the fluorescence after the addition of the quenching species, K_s is the Stern–Volmer quenching constant, and $[C]$ is the concentration of the quencher.

Figure 2 shows the "off-on" principle of g-CNQDs for Ag^+ and Cl^-[21,22]. The nitrogen-containing heterocyclic ring of g-CNQDs makes it fluorescent, and the emission peak is 440 nm at an excitation wavelength of 325 nm, which is in the blue light band. When Ag^+ ions are added, g-CNQDs act as a charge donor and Ag^+ ions act as a charge acceptor, and the charge of the g-CNQDs is transferred to the empty orbital unfilled by Ag^+ via the photoinduced electron transfer (PET) mechanism, and the fluorescence is quenched[23]. Introducing Cl^- ions causes a strong binding affinity between Cl^- ions and Ag^+ ions, leading to the separation of the Ag^+ ions from the surface of the g-CNQDs. This causes the g-CNQDs to return to a monodispersed free state, and fluorescence is restored.

As shown in Fig. 3, the fiber probe was prepared using the following steps, and through these steps, the final result is a fiber probe coated with quantum-doped hydrogel on the side of the fiber.

Step 1: Chemical etching of the optical fibers. First, the cone fiber tip was etched using the Turner method. The fiber end (2 cm in length) was stripped using the mechanical method and cut a flat end face with a cutting knife. Then, the fiber was inserted into the etching solution, which was a 40% HF solution with a thin layer of paraffin protection solution for 70 min. The HF solution can reduce the diameter of the fibers, and the paraffin protective layer prevents the fibers from being etched, resulting in a cone fiber tip. Finally, the fiber was fully washed with ethanol and Milli-Q water.

Step 2: Fiber hydroxy-amination. The fiber tip was immersed in a piranha solution for 30 min, thoroughly cleaned with Milli-Q water, and finally dried for 1 h to complete the fiber hydroxylation. Then the hydroxylated fiber was incubated in a solution of APTES for 5 h to further ammoniate the surface and then thoroughly rinsed with ethanol.

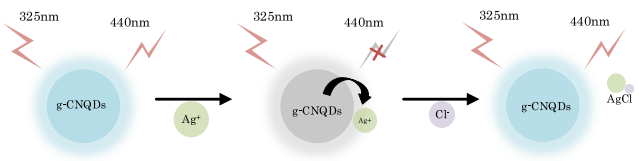

Fig. 2. Schematic of the fluorescence detection of chloride ions by g-CNQDs.

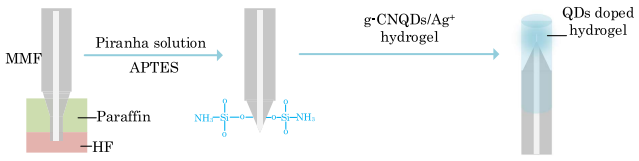

Fig. 3. Schematic of the fiber probe preparation process.

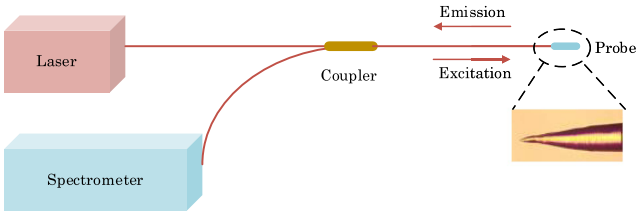

Fig. 4. Schematic of experimental setup.

Step 3: The prepared optical fiber was placed in the lifting machine, the lifting was repeated ten times, and the optical fiber probe containing the fluorescent composite material was cured by heating it at 45°C in a drying oven for 1 h.

To examine the correlation between the fluorescent intensity of the fiber probe and chloride ions, the experimental apparatus schematic is depicted in Fig. 4. The experimental apparatus for reflection spectrum monitoring consists of a spectrometer (AVASPEC-2048, 200–1100 nm) to read the spectrum, a 1×2 50/50 single multimode coupler, and a light source (AvaLight-DHS-BAL). The light source enters the fiber probe through the single multimode fiber coupler, and excited light propagates within the optical fiber probe through total internal reflection, forming an evanescent wave field with an effective penetration depth of tens of nanometers on the surface, stimulating the g -CNQDs on the sensitive film to emit fluorescence. The fluorescence signal is coupled back to the optical fiber probe, which is collected and transmitted by the optical fiber of the single-mode multi-mode optical fiber coupler and then received and processed by the spectrometer. The fiber optic probe is situated within the 3D-printed air chamber with an inlet and outlet, and the chloride ion concentration in the chamber is changed from 1 to 9 μM by an ultrasonic humidifier.

3. Results and Discussion

The fluorescence and absorption characteristics for g-CNQDs/Ag^+ were measured to understand the optical properties of g-CNQDs/Ag^+. Figure 5(a) displays the emission spectra of fluorescence for quantum dots at different excitation wavelengths (315–395 nm). The excitation wavelengths are 315 and 325 nm, the emission wavelength for the g-CNQDs/Ag^+ is 440 nm, and the fluorescence intensity at 325 nm is higher than the fluorescence intensity at 315 nm. The excitation wavelengths are 335–385 nm, although the fluorescence intensity does not change much from that at the excitation wavelength of 325 nm, the new fluorescence peak appears, and the emission wavelength is slightly red-shifted as the excitation wavelength increases. As the excitation wavelength is 395 nm, the fluorescence intensity of the emission peak decreases. Therefore, in the experiment to test the optical properties, the excitation wavelength is 325 nm, and the emission wavelength is 440 nm.

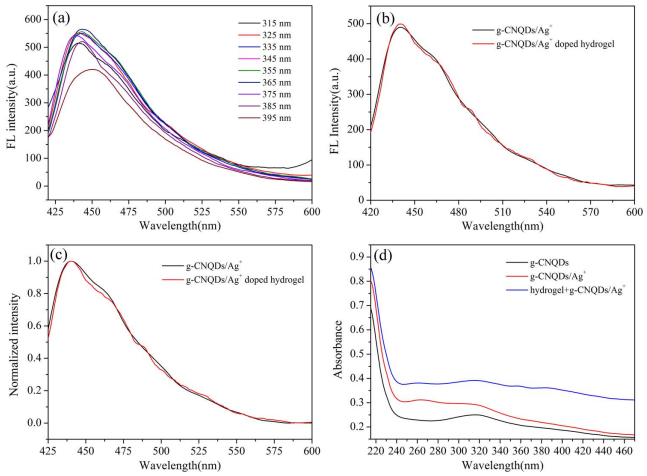

Fig. 5. (a) Different excitation wavelength fluorescence (FL) spectra. (b) Fluorescence spectra for g-CNQDs/Ag^+ and g-CNQDs/Ag^+ within hydrogel. (c) Normalized fluorescence spectra for g-CNQDs/Ag^+ and g-CNQDs/Ag^+ within hydrogel. (d) Absorption spectra for g-CNQDs, g-CNQDs/Ag^+, and g-CNQDs/Ag^+ within hydrogel.

Figure 5(b) shows the fluorescence spectra for g-CNQDs/Ag^+ and the g-CNQDs/Ag^+ added to the hydrogel. After adding the hydrogel, the fluorescence intensity of the emission spectrum was slightly enhanced. After normalization, the fluorescence intensity after normalization is the same, and the emission wavelength is not shifted, as shown in Fig. 5(c). Therefore, the increase in fluorescence intensity is negligible within the error range, i.e., the addition of hydrogel does not affect the emission peak wavelength and the intensity of fluorescence for the g-CNQDs/Ag^+. In Fig. 5(d), the UV absorption spectra for the g-CNQDs, g-CNQDs/Ag^+, and g-CNQDs/Ag^+ hydrogel are shown. The absorption peak is observed at 310 nm due to the $n-\pi^*$ transition of the nitrogen atoms to the unsaturated amino groups, and the g-CNQDs/Ag^+ hydrogel has a higher optical loss due to the absorption of the embedded quantum dot by the hydrogel. The addition of the hydrogel network does not induce a wavelength shift in the absorption peak of the quantum dot.

Figure 6 shows the fluorescence spectra for the quantum dots with the addition of silver ions. As illustrated in Fig. 6, silver ions have a quenching effect on the g-CNQDs. After the silver ions are added, the emission wavelength experiences a 1 nm shift at the excitation wavelength, which may be caused by the decrease of microenvironment polarity, the solvent molecular polarizability, and Stokes shift, leading to the blue shift of the fluorescence peak. The intensity of the fluorescence for the quantum dots progressively decreases as the concentration of silver ions increase.

The influence of the pH on the fiber probe is further analyzed. The fiber probe is placed in different pH solutions within the pH range of 2–10. As illustrated in Fig. 7, the fluorescence intensity varies with the pH in the pH range of 2–10, but the intensity of the fluorescence for the probe exhibits a sharp decrease as the pH is in an alkaline environment (pH = 8–10). The reason

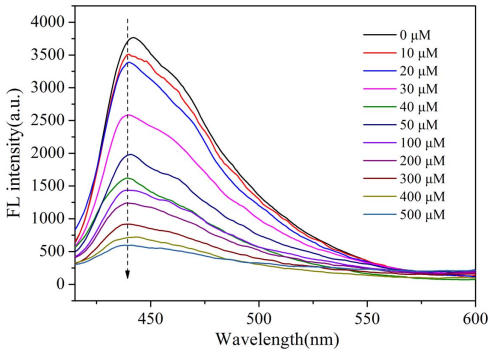

Fig. 6. Fluorescence spectra of Ag^+ added g-CNQDs.

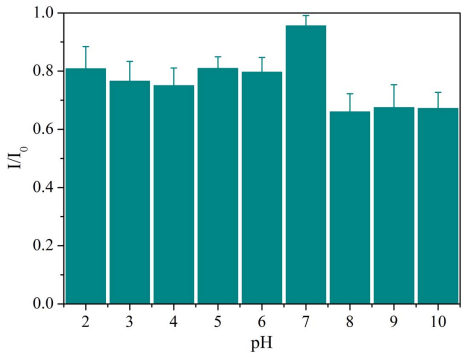

Fig. 7. pH effect on the fluorescence intensity of the fiber probe.

may be that under alkaline conditions, rapid non-radiating electron-hole recombination significantly reduces the population of excited states, thereby quenching the fluorescence[24]. Considering the pH influence on the fluorescence for the g-CNQDs/Ag^+, we chose neutral (pH = 7) for stable chloride ion detection.

To verify the sensitivity of the chloride ion fluorescence detection, the fiber optic probe was placed in an environment where the chloride ion concentration varied from 1 to 9 μM. The fluorescence spectrum of the fiber optic probe in the chloride ion concentration range is illustrated in Fig. 8(a). As the concentration of the chloride ions increases, the strong force between the chloride ion and the silver ion separates the silver ion from the g-CNQDs, which results in partial fluorescence recovery for the g-CNQDs and therefore enhances fluorescence intensity.

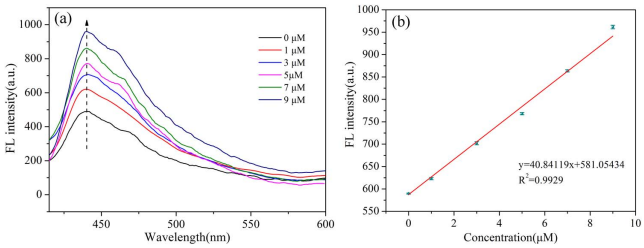

Fig. 8. (a) Fluorescence spectra for optical fiber probes with different chloride ion concentrations. (b) Chloride ion linear fit of fluorescence intensity.

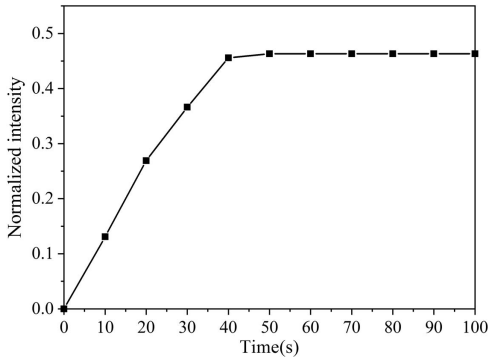

Fig. 9. Fluorescence intensity at different time.

With increasing Cl^- concentration from 1 to 9 μM, the fluorescence intensity of the g -CNQDs increased. Figure 8(b) is a linear fit of the fluorescence intensity (I) and Cl^- concentration. From Fig. 8(b), it can be seen that there exists a robust linear correlation between the intensity of the fluorescence, the concentration of the chloride ion within the range of 1–9 μM, and the correlation coefficient R^2 of 0.9929. The equation of the linear regression is $y = 40.84119[Cl^-] + 581.054334$. When the signal-to-noise ratio (SNR) is 3 times, the corresponding limit of detection (LOD) may be estimated to be 0.037 μM. From Fig. 8(b), it can be seen that after three experiments, there is an error in the experimental data, but the error is small and therefore the sensor has good repeatability. There are two main reasons for the measurement errors. One may be due to the unstable output light intensity of the light source and the other may be affected by temperature.

Figure 9 illustrates the intensity of fluorescence for the fiber probe at different time. The optical fiber probe was placed in a chloride ion environment with a concentration of 5 μM, and the spectral data was recorded every 10 s. As shown in Fig. 9, the response time is 50 s, which means that the diffusion time of chloride ions to the molecules in the hydrogel is 50 s. Response time may vary due to other environmental factors.

Because the main anions in the ocean are nitrate ions, nitrite ions, and sulfate ions, an interference experiment was conducted to explore the influence of other anions on chloride ion detection. As can be seen from Fig. 10, the fluorescence of the

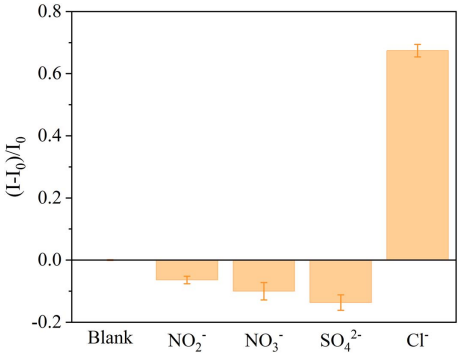

Fig. 10. Fluorescence response to different anions.

Table 1. Compared with Other Materials for Cl^- Detection.

Material	Detection mechanism	R^2	LOD (μM)
6-Methoxy quinoline compound[25]	collision quenching	0.989	15
N,N′-bis (N-benzyl quinolinium) pyridine-2,6-dicarboxamide triflate[26]	PET quenching	—	33
Nitrogen-doped graphene quantum dots/Ag^+[27]	Off-on	0.9899	0.1
This paper	Off-on	0.9929	0.037

g-CNQDs containing Ag^+ is not recovered, and fluorescence quenching occurrs when anions such as nitrate, nitrite, and sulfate are added, while the addition of chloride ions leads to partial recovery of the fluorescence. The reason may be that chloride ions and silver ions have a strong force, can form a complex, restore fluorescence, and other anions and carbon nitride between charge transfer, resulting in the fluorescence quenching phenomenon. It can be assumed that the selectivity for the g-CNQDs of the chloride ions may be attributed primarily to substantial constant stability between the silver ions and the chloride ions. When chloride ions are in excess, silver ions can be pulled out of the g-CNQDs, thus restoring the g-CNQD's fluorescence.

As shown in Table 1, the mechanism R^2 and LOD of the different materials were compared. The sensitive material proposed in this study has several advantages. There is a strong correlation between fluorescence intensity and chloride ions, and the material has a low detection limit. This demonstrates its ability to accurately and reliably detect low concentrations of chloride ions. In order to improve the performance of this sensing optical fiber probe, the structure of the optical fiber probe can be optimized to improve the detection performance of the sensor using a combined conical structure or the performance can be improved by optimizing the material.

4. Conclusion

In summary, we fabricated a g-CNQDs/Ag^+ fluorescent fiber chloride ion sensor based on the "off-on" mechanism. The functional g-CNQDs/Ag^+ are fixed in the hydrogel and partially fluoresced by chloride ions that permeate the hydrogel. When the chloride ion concentration changes, the fluorescence intensity for the g-CNQDs continues to partially recover. The experimental results show that there is a good linearity in the 1–9 μM chloride ion concentration range, and the detection limit is 0.037 μM. The relationship between the intensity of the g-CNQDs/Ag^+ and the concentrations of the chloride ion followed the Stern–Volmer equation, a linear relationship formula of $y = 40.84119[Cl^-] + 581.054334$, and the correlation

coefficient R^2 of 0.9929. The fluorescence sensor has the benefits of convenient and easy manufacture and low production cost. The high-sensitivity fluorescent probe has the advantages of simple structure and easy fabrication.

Acknowledgements

This work was supported by the National Key Research and Development Program of China (No. 2019YFC1407900) and the Natural Science Foundation of Hebei Province (No. F2021203058).

References

1. P. Lebecque, A. Leonard, K. De Boeck, *et al.*, "Early referral to cystic fibrosis specialist centre impacts on respiratory outcome," J. Cyst. Fibros **8**, 26 (2009).
2. S. Toscano, G. La Fornara, and D. Romano, "Salt spray and surfactants induced morphological, physiological, and biochemical responses in callistemon citrinus (Curtis) Plants," Horticulturae **8**, 261 (2022).
3. D. Sweeney, G. Granade, M. Eversmeyer, *et al.*, "Phosphorus, potassium, chloride, and fungicide effects on wheat yield and leaf rust severity," J. Plant Nutr. **23**, 1267 (2000).
4. J. Bujes-Garrido and M. J. Arcos-Martinez, "Development of a wearable electrochemical sensor for voltammetric determination of chloride ions," Sens. Actuators B: Chem. **240**, 224 (2017).
5. Y. Noguchi, L. Zhang, T. Maruta, *et al.*, "Simultaneous determination of fluorine, chlorine and bromine in cement with ion chromatography after pyrolysis," Anal. Chim. Acta **640**, 106 (2009).
6. T. Dietz, J. Klose, P. Kohns, *et al.*, "Quantitative determination of chlorides by molecular laser-induced breakdown spectroscopy," Spectroc. Acta B **152**, 59 (2019).
7. Y. Ma, X. F. Shen, F. Liu, *et al.*, "Colorimetric detection toward halide ions by a silver nanocluster hydrogel," Talanta **211**, 120717 (2020).
8. J. Meija, A. M. Michaowska-kaczmarczyk, and T. Michaowski, "Mohr's method challenge," Anal. Bioanal. Chem. **408**, 1721 (2016).
9. J. Kim, S. Lee, S. Kim, *et al.*, "Development of a fluorescent chemosensor for chloride ion detection in sweat using Ag+-benzimidazole complexes," Dyes Pigments **177**, 108291 (2020).
10. J. Yue, L. Yu, L. Li, *et al.*, "One-step synthesis of green fluorescent carbon dots for chloride detecting and for bioimaging," Front. Chem. **9**, 718856 (2021).
11. T. Gunnlaugsson, A. P. Davis, J. E. O'Brien, *et al.*, "Fluorescent sensing of pyrophosphate and bis-carboxylates with charge neutral PET chemosensors," Org. Lett. **4**, 2449 (2002).
12. J. M. Suk and K. S. Jeong, "Indolocarbazole-based foldamers capable of binding halides in water," J. Am. Chem. Soc. **130**, 11868 (2008).
13. Y. Li and A. Flood, "Pure C-H hydrogen bonding to chloride ions: a preorganized and rigid macrocyclic receptor," Angew. Chem. Int. Ed. **47**, 2649 (2008).
14. W. Xiao, L. Ding, J. He, *et al.*, "Preparation of lucigenin-doped silica nanoparticles and their application in fiber optic chloride ion sensor," Opt. Mater. **98**, 109467 (2019).
15. L. Y. Ding, Z. J. Li, Q. J. Ding, *et al.*, "Microstructured optical fiber based chloride ion sensing method for concrete health monitoring," Sens. Actuat. B **260**, 763 (2018).
16. Y. Tang, Y. Su, N. Yang, *et al.*, "Carbon nitride quantum dots: a novel chemiluminescence system for selective detection of free chlorine in water," Anal. Chem. **86**, 4528 (2014).
17. J. Chen, Y. Gao, X. Hu, *et al.*, "Detection of hydroquinone with a novel fluorescence probe based on the enzymatic reaction of graphite phase carbon nitride quantum dots," Talanta **194**, 493 (2019).
18. L. Liu, J. W. Jin, L. Y. Duan, *et al.*, "Graphitic carbon nitride nanosheets-based turn-on fluorescent biosensor for highly sensitive, label-free detection of adenylate kinase activity," Sens. Actuat. B **8**, 231 (2018).
19. G. Shiravand, A. Badiei, and G. M. Ziarani, "Carboxyl-rich g-C3N4 nanoparticles: Synthesis, characterization and their application for selective fluorescence sensing of Hg2+ and Fe3+ in aqueous media," Sens. Actuat. B **242**, 244 (2017).
20. Y. Xiong, J. Tan, C. Wang, *et al.*, "A miniaturized evanescent-wave free chlorine sensor based on colorimetric determination by integrating on optical fiber surface," Sens. Actuat. B **245**, 674 (2017).
21. H. Liu, X. Wang, H. Wang, *et al.*, "Synthesis and biomedical applications of graphitic carbon nitride quantum dots," J. Mat. Chem. B **7**, 5432 (2019).
22. W. Wei, J. Fan, Y. Xia, *et al.*, "Multi-mode fluorescence sensing detection based on one core-shell structure quantum dots via different types of mechanisms," Spectroc. Acta **241**, 118630 (2020).
23. J. R. Lakowicz, *Principles of Fluorescence Spectroscopy* (Springer, 1983).
24. Z. Zhou, X. Niu, L. Ma, *et al.*, "Revealing the pH-dependent photoluminescence mechanism of graphitic C3N4 quantum dots," Adv. Theory Simul. **2**, 1900074 (2019).
25. C. Ma, F. Zhang, Y. Wang, *et al.*, "Synthesis and application of ratio fluorescence probe for chloride," Anal. Bioanal. Chem. **410**, 6507 (2018).
26. I. J. Bazany-Rodriguez, D. Martinez-Otero, J. Barroso-Flores, *et al.*, "Sensitive water-soluble fluorescent chemosensor for chloride based on a bisquinolinium pyridine-dicarboxamide compound," Sens. Actuat. B **221**, 1348 (2015).
27. X. Fan, S. Wang, Z. Li, *et al.*, "A novel fluorescence sensor for the detection of chloride ion in artificial sweat and environmental water with nitrogen-doped graphene quantum dots," Quim. Nova **45**, 48 (2021).